HHS Public Access

Author manuscript

Curr Biol. Author manuscript; available in PMC 2017 November 07.

Published in final edited form as:

Curr Biol. 2016 November 7; 26(21): 2957–2965. doi:10.1016/j.cub.2016.08.066.

Phosphorylation of the polarity protein BASL differentiates asymmetric cell fate through MAPKs and SPCH

Ying Zhang[1], **Xiaoyu Guo**[1], and **Juan Dong**[1,2,*]

[1]The Waksman Institute of Microbiology, Rutgers the State University of New Jersey, Piscataway, NJ 08854, USA

[2]Department of Plant Biology and Pathology, Rutgers the State University of New Jersey, Piscataway, NJ 08901, USA

SUMMARY

Cell polarization is commonly used for the regulation of stem cell asymmetric division in both animals and plants. Stomatal development in *Arabidopsis*, a process that produces breathing pores in the epidermis, requires asymmetric cell division to differentiate highly specialized guard cells while maintaining a stem cell population [1, 2]. The BREAKING OF ASYMMETRY IN THE STOMATAL LINEAGE (BASL) protein exhibits a polarized localization pattern in the cell and is required for differential cell fates resulting from asymmetric cell division [3]. The polarization of BASL is made possible by a positive feedback loop with a canonical Mitogen-activated protein kinase (MAPK) pathway that recruits the MAPKK Kinase YODA (YDA) and MAPK 6 (MPK6) to the cortical polarity site [4]. Here we study BASL intracellular dynamics and show that the membrane-associated BASL is slowly replenished at the cortical polarity site and the mobility is tightly linked to its phosphorylation status. Because BASL polarity is only exhibited by one daughter cell after an asymmetric cell division, we study how BASL differentially functions in the two daughter cells. The YDA MAPK cascade transduces upstream ligand-receptor signaling [5–13] to the transcription factor SPEECHLESS (SPCH) that controls stomatal initiation and is directly suppressed by MPK3/6-mediated phosphorylation [14, 15]. We show that BASL polarization leads to elevated nuclear MPK6 signaling and lowered SPCH abundance in one of the two daughter cells. Therefore, two daughter cells are differentiated by BASL polarity-mediated differential suppression of SPCH, which may provide developmental plasticity in plant stem cell ACD.

Graphical Abstract

Contact: dong@waksman.rutgers.edu.

AUTHOR CONTRIBUTIONS

This study was designed by J.D. and Y.Z.; Y.Z. and X.G. performed the experiments; Y.Z. and J.D. analyzed the data; J.D. and Y.Z. wrote the paper.

COMPETING FINANCIAL INTEREST

The authors declare no competing financial interests.

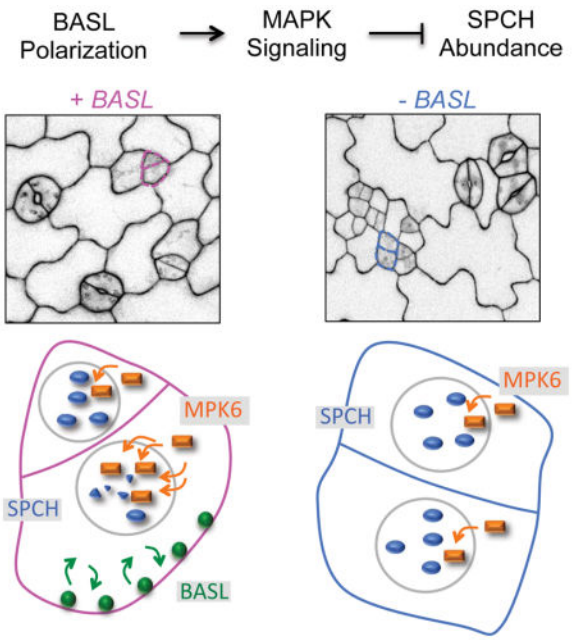

Keywords

Cell polarity; asymmetric cell fate; stomatal development; FRAP; polarity protein; MAPK dynamics; transcription factor degradation

RESULTS

Low Mobility of BASL at the Cortical Polarity Site

The plant-specific protein BASL regulates stomatal division asymmetries mainly *via* its highly polarized localization to the cell cortex of asymmetric cell division (ACD) precursors [3] (Figure 1A, green). Polarization of BASL at the cell cortex mirrors that of the conserved polarity proteins Partitioning defective (PARs) in *Drosophila* and *C. elegans* [16], but differs in its nuclear accumulation (Figure 1A). Loss of *BASL* leads to failures in stomatal ACD; the mutants are featured with symmetric lineage cell divisions and clustered guard cells (Figure 1B)[3].

To understand the membrane-associated BASL's intracellular dynamics, we conducted fluorescence recovery after photobleaching (FRAP) [17]. The fusion protein driven by the endogenous promoter fully complements *basl* loss-of-function mutants [3]. FRAP on GFP-BASL at the polarity site showed obvious recovery within 10-min of monitoring (Figure S1A) and almost plateaued at about 20-min (Figure S1B). To test whether heterogeneous cytoplasmic substances may locally affect BASL's mobility, we monitored three small segments along the plasma membrane (PM) and found that each segment recovered similarly (n = 3 cells) and the average mirrored the full-length recovery (Figure S1C). The kymograph of the full-length crescent also suggested relative even recovery along the periphery with more enrichment in the center (Figure S1D). Thus, the full-length FRAP recoveries were generally assayed for BASL and other proteins in this study. The cortical

region is referred as *FRAP SLGC "polar" site* for the figures. By an Exponential curve-fitting approach, we normalized the raw intensity data (Figure S1A) to determine the relative recovered rate during 600-sec after bleaching (Figure 1C and Table S1 for R^2). The slow but steady recovery of GFP-BASL (I_{600} = 38.60% at 600-sec, n = 5 representative cells) is strikingly distinct from fast recovery of the small GTPase GFP-ROP2 (Figure S1E), a molecular switch of cell polarity in plants [18], but surprisingly resembles that of the membrane-embedded PIN3-GFP protein (Figure S1E). On the other hand, FRAP on the nuclear pool of GFP-BASL did not show obvious recovery (Figure 1C, I_{600} = 6.77%), suggesting a static status of nuclear BASL.

Many models for polarization require protein movement on and off the membrane [19, 20]. By taking advantage of the myristoylation (myr) modification that irreversibly attaches target protein to the PM [21], we tested BASL mobility along the PM. Interestingly, Myr-GFP-BASL maintained polar distribution at the PM (Figure 1D) and rescued *basl-3* mutants effectively [22], suggesting that tight association of BASL with the PM is capable of forming polarity. *basl-3* is comparable to *basl-2* in producing stomatal phenotype (Figure S1F) [22], but the T-DNA insertion confers a more convenient antibiotic selection; therefore the two alleles were used interchangeably in this study. We compared FRAP recovery and showed the polar pool was less mobile than the non-polar pool (Figure 1D, polar I_{600} = 21.71% *vs*. non-polar 41.02%), suggesting the active molecules (polar) are less dynamic than the inactive ones (non-polar) even when modified by myristoylation.

Phosphorylation Status Changes BASL Mobility at the Cell Cortex

We previously reported that BASL contains six putative phosphorylation sites (SerPro, S1–S6 in Figure 1A) with five being MPK6 substrate, and all six sites seem to be important for BASL polarization and function [4]. We further asked whether and how phosphorylation regulates BASL mobility. We first conducted FRAP on two modified forms of BASL. One represents a high phosphorylation form (GFP-BASL_123456D) with all six SP (SerPro) sites mutated to phospho-mimicking DPs (AspPro), which fully rescued *basl* and showed polarity comparable to that of GFP-BASL (Figure 1E and S2A) [4]. The other one represents a low phosphorylation form (GFP-BASL_12356A) with five SPs mutated to phospho-deficient APs (AlaPro) that displayed disrupted polarity and function (Figure 1E and S2A) [4]. The previously reported GFP-BASL_123456A with all six SP sites mutated to APs is restricted in the nucleus [4], therefore cannot be used for cortical FRAP. Our data showed that at the cell cortex GFP-BASL_12356A is more mobile (Figure 1E, I_{600} = 51.88%) than GFP-BASL (I_{600} = 38.11%) and GFP-BASL_123456D (I_{600} = 30.74%). This suggests that phosphorylation status of BASL might influence its cortical mobility. However, phosphorylation status did not change BASL immobility in the nucleus (Figure S1G).

Although transgenic BASL variants are expressed similarly at the transcript level (Figure S2D), we assessed whether the protein abundance and stability at cellular level, in particular at the FRAP region may affect FRAP curves. The GFP-BASL intensity varies in individual cells even in a single leaf (Figure S1H). We bleached the cells expressing high level of GFP (absolute intensity at the SLGC "polar" site > 110 pixels) to compare with the ones with low levels (< 80 pixels, n = 6, Table S2) and found they recovered very similarly (Figure S1H).

To examine protein stability, we treated plants with Cycloheximide (CHX) to inhibit protein synthesis followed by monitoring absolute GFP intensity for 10-min. The results show that no obvious protein degradation were detected within the 600-sec FRAP duration among all the transgenic lines we examined (Figure S1I). Thus, the FRAP differences of BASL variants likely reflect their molecular property and function, but are not significantly related to protein abundance and degradation.

We further explored other phospho-variants of BASL and surveyed their mobility at the cell cortex (data not shown). Interestingly, GFP-BASL_14D (S1 and S4 were mutated to Asp, D) showed severely retarded recovery at the cell cortex (Figure 1E, I_{600} = 17.02% *vs*. GFP-BASL 38.11%). The protein abundance and stability of GFP-BASL_14D at the polarity site are comparable to those in WT (Figure S1I).

BASL_14D Shows Enhanced Activity

Intrigued by the strikingly lowered mobility of GFP-BASL_14D, we further characterized its subcellular localization and function in plants. GFP-BASL_14D is primarily found at the cell cortex (Figure 2A) and accumulates very weakly in the nuclei of a small number of cells (Figure S2B, 30-hpg, 24.3% in 70 GFP-positive cells *vs*. WT 96.2% n = 52). Polarized GFP-BASL_14D displayed prolonged protein accumulation even in mature pavement cells (5-dpg, Figure S2C).

GFP-BASL_14D also produced an unexpected stomatal phenotype. Quantification of stomatal index (SI = total number of stomata/total number of epidermal cells × 100%) in a homozygous population harboring one copy of the transgene (see Experimental Procedures and transcript level evaluated in Figure S2D) showed that GFP-BASL_14D not only rescued stomatal overproduction in *basl-3*, it further suppressed stomatal formation (Figure 2B, BASL_14D SI = 14% *vs*. 23% of BASL). The phenotype of BASL_14D cannot be recapitulated by overexpressing GFP-BASL (quantification in Figure 2B), which showed similarly prolonged expression in pavement cells (Figure S2C).

We further investigated at what developmental stage GFP-BASL_14D affected stomatal production. At the initiation stage (2-dpg seedlings), BASL_14D produced a slightly reduced number of stomatal precursor cells (Figure 2C). At later stages, the M spiral divisions typically produce one stoma surrounded by three pavement cells and the SLGC spacing division produces two stomata separated by one cell (Figure 2D). Interestingly, GFP-BASL_14D did not change the typical spiral division of Ms (Figure 2E), but drastically suppressed the SLGC spacing divisions (Figure 2F). In most cases, the SLGCs in GFP-BASL_14D expand without producing another round of division (Figure 2F, light blue). These results support that BASL_14D negatively impacts on stomatal production mainly *via* suppressing the SLGC division potential (Figure 2D).

Differential MAP Kinase Dynamics in Stomatal ACD Cells

The positive feedback loop between BASL and the YDA MAPK pathway led to co-polarization of YDA and MPK3/6 with BASL in stomatal ACD cells (Figure 1A)[4]. It was hypothesized that SLGCs inherit the polarity complex and differ from Ms by a concentrated MAPK signaling activity [4]. Here, we performed FRAP analyses to examine the mobility,

possibly reflective of its signaling activity, of MPK6 in two daughter cells. We first tested the feasibility of FRAP in revealing MAPK mobility and activity by photobleaching YFP-tagged proteins in the nucleus of mature tobacco epidermal cells, a relatively pure cell system without intensive developmental regulations. A kinase-dead version of MPK6 (MPK6_AEF-YFP; the conserved catalytic loop TEY amino acids mutated to AEF)[23] was used as a negative control. Based on our FRAP data, MPK6 was more mobile than MPK6_AEF (I_{300} = 81.37% *vs.* 67.37% respectively, n = 6) (Figure S3A). Furthermore, H_2O_2, a stimulant of the MPK6 signaling in plant cells [24] elevated the mobility of MPK6-YFP (I_{300} from 81.37% to 94.4%, n = 5). In contrast, application of a MAPK inhibitor (U0126) [25] suppressed it (I_{300} from 79.15% for the DMSO mock to 57.75%, n = 6) (Figure S3A). These results indicate that FRAP can be used as a sensitive tool to measure the intracellular dynamics of MPK6 in plant cells.

For *in vivo* examination, MPK6-mRFP (driven by the *BASL* promoter) was expressed in *Arabidopsis* stomatal lineage cells (Figure 3A). When plants were treated with the activator H_2O_2, nuclear MPK6-mRFP mobility was increased (Figure 3B, from I_{300} = 41.95% to 53.66% in SLGCs), consistent with our tobacco data. To evaluate MPK6 mobility in two ACD daughter cells, we generated FRAP curves for nuclear MPK6-mRFP in SLGCs and in Ms, respectively. Interestingly, MPK6-mRFP recovered differentially (Figure 3B); it is more mobile in SLGCs (I_{300} = 41.95%, n = 5) than in Ms (I_{300} = 32.62%). The differential mobility (DM) of MPK6 between SLGCs and Ms is about 28.58% (Figure 3C, n = 5 pairs) and appears to depend on BASL. In *basl*-2, this difference is diminished (Figure 3C, DM = 0.97%). We expanded this analysis to MPK6-mRFP co-expressed with Myr-GFP-BASL and GFP-BASL_14D, respectively, and found that MPK6 consistently shows relative high mobility in the SLGCs (Figure 3D and S3D). Importantly, the super active GFP-BASL_14D greatly enhanced this difference (Figure 3C, DM = 79.36%).

To further evaluate whether MPK6 kinase activity is elevated by BASL polarization, we examined the activity level of MPK3 and MPK6 by using a p44/42 MAPK antibody in different *BASL* backgrounds. Interestingly, an obvious elevation of MPK6 activity was found in the plants expressing the super active form GFP-BASL_14D (Figure 3E). Taken together, these results indicate that polarized BASL positively contributes to elevated MPK6 signaling activity.

As a negative control, MPK6_AEF-mRFP resembled that of MPK6_mRFP in subcellular localization (Figure S3C), but its expression induces clustered stomata (Figure S3B) as seen in the loss-of-function mutants [6]. Our FRAP results showed that MPK6_AEF-mRFP displayed lowered recoveries (Figure S3C, I_{300} = 25.83%). Importantly, the presence of *BASL* did not contribute to an obvious mobility change for MPK6_AEF (I_{300} = 26.50% in *basl-2*, n = 5 pairs), which is in contrast to how BASL increased MPK6 mobility (Figure S3C).

Low SPCH Levels Are Associated with BASL Polarity

The bHLH transcription factor SPCH is the master regulator of stomatal lineage initiation [15] and a direct substrate of MPK3 and MPK6 in the nucleus for degradation. This is supported by the previous publication [14] and the more restricted expression pattern of

SPCH translational fusion than that of the transcriptional fusion (Figure S4A). BASL cortical polarization was proposed to associate with high MAPK signaling and low SPCH levels in SLGCs [4]. To test this hypothesis, we first characterized the genetic interaction. Introducing an extra copy of SPCH (*SPCHpro*::SPCH-CFP) in WT plants induced an elevated stomatal index and this phenotype is suppressed by an extra copy of BASL (Figure 4A, expression levels of SPCH-CFP were evaluated in Figure S4B). The introgression of GFP-BASL_14D further suppressed the SPCH-CFP phenotype (Figure 4A), suggesting that SPCH activity is constrained by polarized BASL.

We further examined the protein level of SPCH in relation to BASL polarity in stomatal ACD pairs by measuring the nuclear fluorescence intensity of SPCH-CFP (Figure 4B). We found that in the cells expressing both markers, SPCH accumulated less in the SLGCs where BASL is polarized (Figure 4B) while equivalent levels of nuclear GFP-BASL were evident (Figure 4B). The median level of CFP intensity ratio between Ms and SLGCs was 1.71 (Figure 4C, data distribution in Table S3), while in *basl-2*, SPCH-CFP was equally expressed (median = 1.04, Figure 4C and 4D). On the other hand, this difference was elevated by co-expressing GFP-BASL_14D (median = 2.86, Figure 4C and 4E). As SPCH is phosphorylated by MPK3/6 on five Ser sites for degradation [14], expression of a degradation-resistant version SPCH_1-5A-CFP resulted in over-proliferation of stomatal cells (Figure 4F) and, interestingly, failed to show unequal expression in two daughter cells (median = 1.03, Figure 4C and 4F), similar to SPCH-CFP in *basl-2*. Furthermore, introgression of GFP-BASL_14D into SPCH_1-5A did not change this equivalence (median = 1.01, Figure 4C and 4G). This is most likely due to the insensitivity of SPCH_1-5A to BASL polarity-associated high MAPK activity.

DISCUSSION

Polarization of a mother cell is critical for its asymmetric division and subsequent differentiation of two daughter cells, but the molecular mechanisms for the connection are poorly characterized in plants. Our current studies revealed the missing mechanistic link between the plant-specific BASL polarity protein and asymmetric fate specification during stomatal differentiation in *Arabidopsis*.

Elevated MAPK Mobility and Kinase Activity Associated with BASL Polarity

We showed that FRAP assay can be used as a sensitive technique to measure MAPK signaling activity in plant cells. Kinase activities are generally evaluated by radioactively labeled substrates in *in vitro* assays [26], but can barely be demonstrated at the subcellular level and in a cell type-specific manner. Here, we used FRAP to demonstrate that because of polarized BASL, MPK6 mobility is unequal between two daughter cells.

MAP kinase dynamics has been better studied in budding yeast [27]. The rapid recovery of MAPK Fus3p in the nucleus was independent of pheromone treatment and the presence of the membrane-bound Ste5p scaffold protein [28]. In contrast, as a MAPK scaffold protein, polarized BASL promoting the nuclear MAPK mobility and activity in stomatal ACD cells becomes remarkable. The elevated mobility of MPK6 in the SLGC most likely results from

concentrated accumulation of the upstream MAPKKK YDA and MPK3/6 at the BASL polarity site [4] that promotes more activated MPK3/6 molecules shuttling into the nucleus.

Based on our FRAP data, we propose a working model for BASL polarization and MAPK dynamics in stomatal lineage cells (Figure S4C). Once imported into the nucleus, BASL becomes relatively immobile. At the cortical polarity site, BASL molecules undergo slow but active replenishment. Polarized BASL in the SLGC promotes fast shuttling of MPK3/6 into the nucleus, which enhances their ability to phosphorylate SPCH for degradation.

Differential SPCH Levels in Two Daughter Cells

Cell fate-determining factors are instrumental for development and require precise spatial control in their expression. In *Drosophila* and vertebrate nervous systems, polarity proteins ensure the conserved cell fate-determining factor NUMB to partition to one of the two progeny cells [29]. In plant development, many transcription factors are spatiotemporally controlled. In *Arabidopsis* early embryogenesis, WOX2 defines the apical lineage domain and WOX8/9 are required for the basal lineage development [30, 31]. The expression of SHOOT ROOT (SHR) and SCARECROW (SCR) are spatially controlled to specify the endodermis identity in the roots [32, 33]. However, BASL polarity seems to function differently in stomatal ACD; it distinguishes two daughter cells through lowering SPCH levels, but not by segregating SPCH production. SPCH function is dosage-dependent [14, 15] and two daughter cells are intrinsically different in their divisional potential [34]. Now this can be explained by the presence of BASL polarity in only one daughter cell. BASL-centered differential suppression of SPCH might represent a specific solution to the plasticity of stomatal development, during which stem cell divisions are constantly modulated by environmental and developmental changes.

Slow Mobility of BASL at the PM

Our FRAP data showed that polarized BASL recovers dramatically slower than the membrane-associated PAR proteins in *C. elegans* [35] and ROP small GTPase in *Arabidopsis* [36] (full recovery achieved within 1-min in both cases). To our surprise, as a non-membrane integral protein, the BASL recovery curve more resembled that of the membrane-embedded PINs and the BOR1 boron transporter (about 30–40% recovery in 20-min) [37, 38]. How BASL is targeted to the PM polarity site is unknown. Based on our FRAP data, it is tempting to propose that BASL interacts with membrane-embedded partner/s that utilize the vesicular trafficking routes for asymmetric localization.

Taken together, our results shed novel lights on the intracellular dynamics of this unique polarity protein in plant cells and provided mechanistic insights into the functions of BASL in differentiating two daughter cells in stomatal ACD.

Supplementary Material

Refer to Web version on PubMed Central for supplementary material.

Acknowledgments

We thank Tijs Ketelaar (Wageningen U.) and Lynn Pillitteri (Western Washington U.) for critical reading of the manuscript. We are grateful for the SPCH-related reagents from Dr. Dominique Bergmann (Stanford U.) and the gateway binary vectors from Dr. Tsuyoshi Nakagawa (Shimane U.). This work is supported by grants from the U.S. National Institute of General Medical Sciences to J.D. (R01GM109080).

References

1. Bergmann DC, Sack FD. Stomatal development. Annual review of plant biology. 2007; 58:163–181.
2. Pillitteri LJ, Torii KU. Mechanisms of stomatal development. Annual review of plant biology. 2012; 63:591–614.
3. Dong J, MacAlister CA, Bergmann DC. BASL controls asymmetric cell division in *Arabidopsis*. Cell. 2009; 137:1320–1330. [PubMed: 19523675]
4. Zhang Y, Wang P, Shao W, Zhu JK, Dong J. The BASL polarity protein controls a MAPK signaling feedback loop in asymmetric cell division. Developmental cell. 2015; 33:136–149. [PubMed: 25843888]
5. Bergmann DC, Lukowitz W, Somerville CR. Stomatal development and pattern controlled by a MAPKK kinase. Science (New York, NY). 2004; 304:1494–1497.
6. Wang H, Ngwenyama N, Liu Y, Walker JC, Zhang S. Stomatal development and patterning are regulated by environmentally responsive mitogen-activated protein kinases in *Arabidopsis*. The Plant cell. 2007; 19:63–73. [PubMed: 17259259]
7. Shpak ED, McAbee JM, Pillitteri LJ, Torii KU. Stomatal patterning and differentiation by synergistic interactions of receptor kinases. Science (New York, NY). 2005; 309:290–293.
8. Nadeau JA, Sack FD. Control of stomatal distribution on the *Arabidopsis* leaf surface. Science (New York, NY). 2002; 296:1697–1700.
9. Abrash EB, Bergmann DC. Regional specification of stomatal production by the putative ligand CHALLAH. Development (Cambridge, England). 2010; 137:447–455.
10. Hara K, Kajita R, Torii KU, Bergmann DC, Kakimoto T. The secretory peptide gene EPF1 enforces the stomatal one-cell-spacing rule. Genes & development. 2007; 21:1720–1725. [PubMed: 17639078]
11. Hara K, Yokoo T, Kajita R, Onishi T, Yahata S, Peterson KM, Torii KU, Kakimoto T. Epidermal cell density is autoregulated via a secretory peptide, EPIDERMAL PATTERNING FACTOR 2 in *Arabidopsis* leaves. Plant & cell physiology. 2009; 50:1019–1031. [PubMed: 19435754]
12. Kondo T, Kajita R, Miyazaki A, Hokoyama M, Nakamura-Miura T, Mizuno S, Masuda Y, Irie K, Tanaka Y, Takada S, et al. Stomatal density is controlled by a mesophyll-derived signaling molecule. Plant & cell physiology. 2010; 51:1–8. [PubMed: 20007289]
13. Sugano SS, Shimada T, Imai Y, Okawa K, Tamai A, Mori M, Hara-Nishimura I. Stomagen positively regulates stomatal density in *Arabidopsis*. Nature. 2010; 463:241–244. [PubMed: 20010603]
14. Lampard GR, Macalister CA, Bergmann DC. *Arabidopsis* stomatal initiation is controlled by MAPK-mediated regulation of the bHLH SPEECHLESS. Science (New York, NY). 2008; 322:1113–1116.
15. MacAlister CA, Ohashi-Ito K, Bergmann DC. Transcription factor control of asymmetric cell divisions that establish the stomatal lineage. Nature. 2007; 445:537–540. [PubMed: 17183265]
16. Goehring NW. PAR polarity: from complexity to design principles. Experimental cell research. 2014; 328:258–266. [PubMed: 25128809]
17. White J, Stelzer E. Photobleaching GFP reveals protein dynamics inside live cells. Trends in cell biology. 1999; 9:61–65. [PubMed: 10087620]
18. Fu Y, Gu Y, Zheng Z, Wasteneys G, Yang Z. *Arabidopsis* interdigitating cell growth requires two antagonistic pathways with opposing action on cell morphogenesis. Cell. 2005; 120:687–700. [PubMed: 15766531]
19. Altschuler SJ, Angenent SB, Wang Y, Wu LF. On the spontaneous emergence of cell polarity. Nature. 2008; 454:886–889. [PubMed: 18704086]

20. Slaughter BD, Smith SE, Li R. Symmetry breaking in the life cycle of the budding yeast. Cold Spring Harbor perspectives in biology. 2009; 1:a003384. [PubMed: 20066112]
21. Martin DD, Beauchamp E, Berthiaume LG. Post-translational myristoylation: Fat matters in cellular life and death. Biochimie. 2011; 93:18–31. [PubMed: 21056615]
22. Zhang Y, Bergmann DC, Dong J. Fine-scale dissection of the subdomains of polarity protein BASL in stomatal asymmetric cell division. Journal of experimental botany. 2016
23. Bush SM, Krysan PJ. Mutational evidence that the *Arabidopsis* MAP kinase MPK6 is involved in anther, inflorescence, and embryo development. Journal of experimental botany. 2007; 58:2181–2191. [PubMed: 17519351]
24. Wang P, Du Y, Li Y, Ren D, Song CP. Hydrogen peroxide-mediated activation of MAP kinase 6 modulates nitric oxide biosynthesis and signal transduction in *Arabidopsis*. The Plant cell. 2010; 22:2981–2998. [PubMed: 20870959]
25. Yoo SD, Cho YH, Tena G, Xiong Y, Sheen J. Dual control of nuclear EIN3 by bifurcate MAPK cascades in C2H4 signalling. Nature. 2008; 451:789–795. [PubMed: 18273012]
26. Kubiak JZ. Protein kinase assays for measuring MPF and MAPK activities in mouse and rat oocytes and early embryos. Methods in molecular biology (Clifton, NJ). 2013; 957:77–89.
27. Van Drogen F, Peter M. MAP kinase dynamics in yeast. Biology of the Cell. 2001; 93:63–70. [PubMed: 11730324]
28. van Drogen F, Stucke VM, Jorritsma G, Peter M. MAP kinase dynamics in response to pheromones in budding yeast. Nature cell biology. 2001; 3:1051–1059. [PubMed: 11781566]
29. Haenfler JM, Kuang C, Lee CY. Cortical aPKC kinase activity distinguishes neural stem cells from progenitor cells by ensuring asymmetric segregation of Numb. Developmental biology. 2012; 365:219–228. [PubMed: 22394487]
30. Breuninger H, Rikirsch E, Hermann M, Ueda M, Laux T. Differential expression of WOX genes mediates apical-basal axis formation in the *Arabidopsis* embryo. Dev Cell. 2008; 14:867–876. [PubMed: 18539115]
31. Ueda M, Zhang Z, Laux T. Transcriptional activation of *Arabidopsis* axis patterning genes WOX8/9 links zygote polarity to embryo development. Dev Cell. 2011; 20:264–270. [PubMed: 21316593]
32. Cui H, Levesque MP, Vernoux T, Jung JW, Paquette AJ, Gallagher KL, Wang JY, Blilou I, Scheres B, Benfey PN. An evolutionarily conserved mechanism delimiting SHR movement defines a single layer of endodermis in plants. Science (New York, NY). 2007; 316:421–425.
33. Helariutta Y, Fukaki H, Wysocka-Diller J, Nakajima K, Jung J, Sena G, Hauser MT, Benfey PN. The SHORT-ROOT gene controls radial patterning of the *Arabidopsis* root through radial signaling. Cell. 2000; 101:555–567. [PubMed: 10850497]
34. Nadeau JA, Sack FD. Stomatal development in *Arabidopsis*. The *Arabidopsis* book/American Society of Plant Biologists. 2002; 1:e0066.
35. Goehring NW, Hoege C, Grill SW, Hyman AA. PAR proteins diffuse freely across the anterior-posterior boundary in polarized C. elegans embryos. The Journal of cell biology. 2011; 193:583–594. [PubMed: 21518794]
36. Sorek N, Segev O, Gutman O, Bar E, Richter S, Poraty L, Hirsch JA, Henis YI, Lewinsohn E, Jurgens G, et al. An S-acylation switch of conserved G domain cysteines is required for polarity signaling by ROP GTPases. Current biology: CB. 2010; 20:914–920. [PubMed: 20451389]
37. Men S, Boutte Y, Ikeda Y, Li X, Palme K, Stierhof YD, Hartmann MA, Moritz T, Grebe M. Sterol-dependent endocytosis mediates post-cytokinetic acquisition of PIN2 auxin efflux carrier polarity. Nature cell biology. 2008; 10:237–244. [PubMed: 18223643]
38. Takano J, Tanaka M, Toyoda A, Miwa K, Kasai K, Fuji K, Onouchi H, Naito S, Fujiwara T. Polar localization and degradation of *Arabidopsis* boron transporters through distinct trafficking pathways. Proceedings of the National Academy of Sciences of the United States of America. 2010; 107:5220–5225. [PubMed: 20194745]

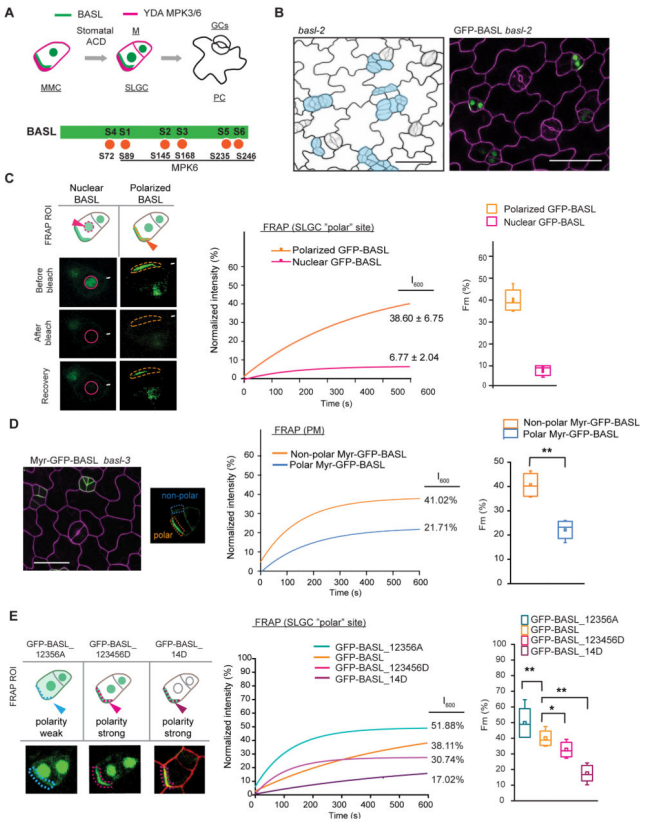

Figure 1. BASL is Mildly Mobile at The Cell Cortex

(A) A schematic diagram shows co-polarization of BASL (green) and YDA-MPK3/6 (magenta) at the cell cortex in stomatal development. MMC, meristemoid mother cell; SLGC, stomatal lineage ground cell; M, meristemoid; GCs, guard cells; PC, pavement cell; ACD, asymmetric cell division. Bottom schematic shows the putative MAPK phosphorylation sites (SerPro, S1–S6) in the BASL protein. Five of them (underlined) are confirmed substrates of MPK6 *in vitro*.

(B) Confocal images show stomatal phenotype of 2-dpg *basl*-2 and GFP-BASL (green) *basl-2*. Light blue highlights abnormal divisions and clustered guard cells in the mutant. Cell walls were stained with propidium iodide (PI) (Magenta) and this applies to all the other figures. Scale bars = 25 μm.

(C) FRAP analyses of nuclear and cortically polarized GFP-BASL, respectively. Photobleaching (arrowheads) were performed at the designated locations. GFP fluorescence intensity were measured (dashed lines in top diagrams) and normalized. The FRAP curve is plotted as a function of time at 5-s intervals (middle). The F_m raw data at time 600-sec were calculated for box plotting and comparison of GFP recovery (right panel). The SLGC cortical regions analyzed for FRAP were referred as SLGC “polar” site in general.

(D) Left: confocal images show localization of Myr-GFP-BASL *basl*-3. The PM regions used for FRAP are highlighted as “non-polar” and “polar”, respectively. Middle: FRAP curves of Myr-GFP-BASL at the polar site (orange) *vs.* at the non-polar site (blue). Right: comparison of GFP recovery between the non-polar and polar pools of Myr-GFP-BASL. Mann–Whitney U test, ** $p < 0.01$.

(E) Comparison of FRAP curves of GFP-BASL and the phospho-variants at the SLGC "polar" site. Note the slow recovery of GFP-BASL_14D. The mobile fractions from raw data (F_m,) were used for statistical comparison. Mann–Whitney U test, * $p < 0.05$, ** $p < 0.01$.

See also Figure S1 and S2, and Table S1 and S2.

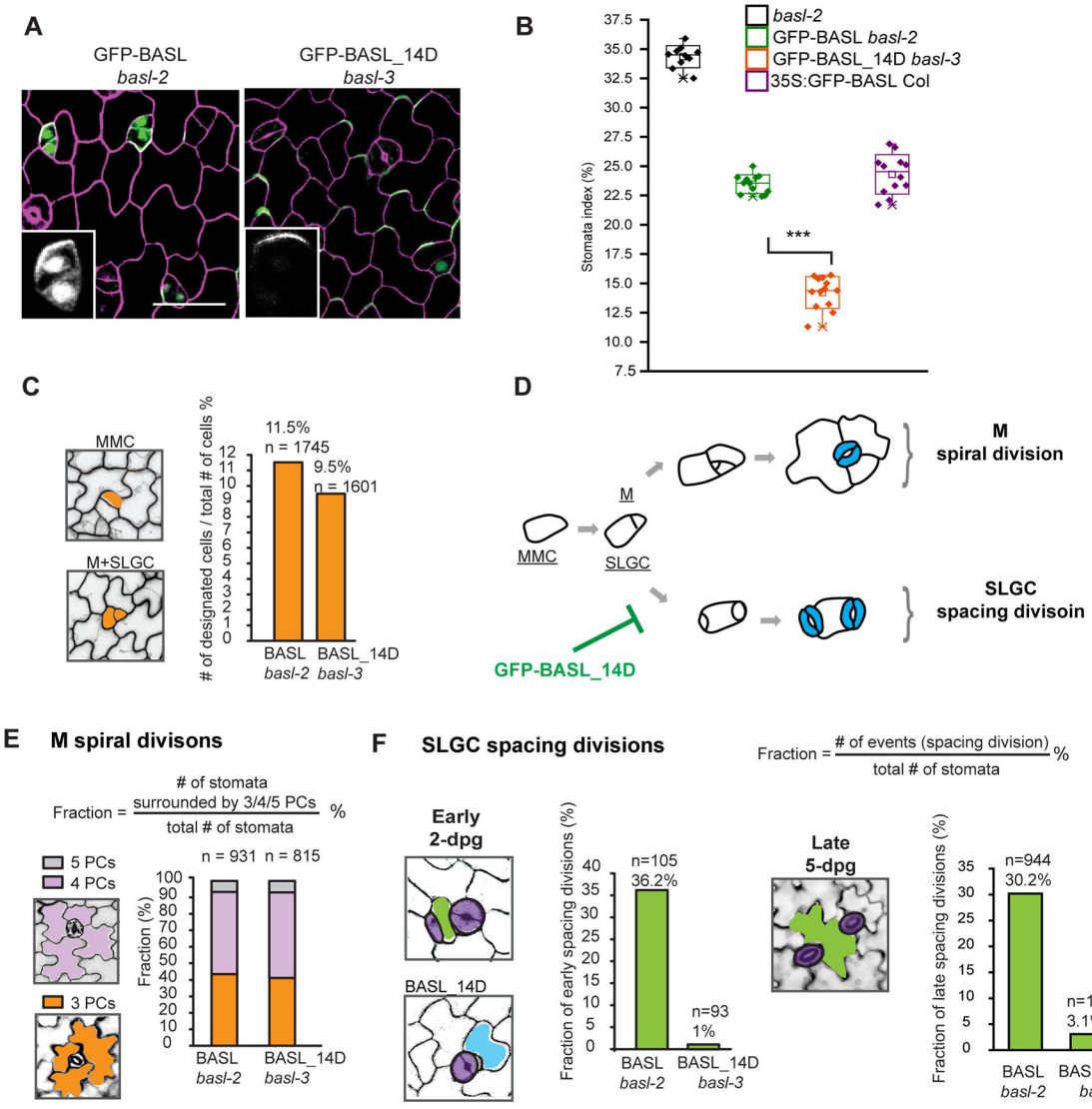

Figure 2. GFP-BASL_14D Suppresses SLGC Spacing Divisions in Stomatal Development

(A) Representative confocal images of GFP-BASL and GFP-BASL_14D (green) in 2-dpg *basl* mutants. Insets show detailed GFP localization (Note BASL_14D is mainly at the PM). Scale bars = 25 μm

(B) Box plots show quantification of Stomatal Index (SI) in 5-dpg adaxial cotyledons. Note GFP-BASL_14D exhibits greatly reduced SI. Mann–Whitney U test, *** $p < 0.0001$.

(C) Left: representative confocal images show stomatal lineage initiation events (highlighted with orange). Right: histograms show the quantification (n = total number of epidermal cells).

(D) Schematic of division patterns of M and SLGC. An M typically divides three times before terminates into a pair of guard cells. A SLGC spacing division produces two stomata separated by one spacing cell. Polarized GFP-BASL_14D suppresses the SLGC spacing divisions (block line).

(E) Histograms show quantification of M spiral divisions in 5-dpg adaxial seedlings. BASL_14D does not change M spiral divisions. The numbers (n) indicate total stomata counted.

(F) Histograms show quantification of SLGC spacing divisions in early (2-dpg, left) and late (5-dpg, right) adaxial cotyledons. BASL_14D strongly suppresses SLGC spacing divisions. Confocal or DIC images show typical spacing divisions of GFP-BASL, two stomatal cells (purple) separated by one non-stomatal cell (green), and an atypical division of GFP-BASL_14D (one blue non-stomatal cell abutting one stoma).

See also Figure S2.

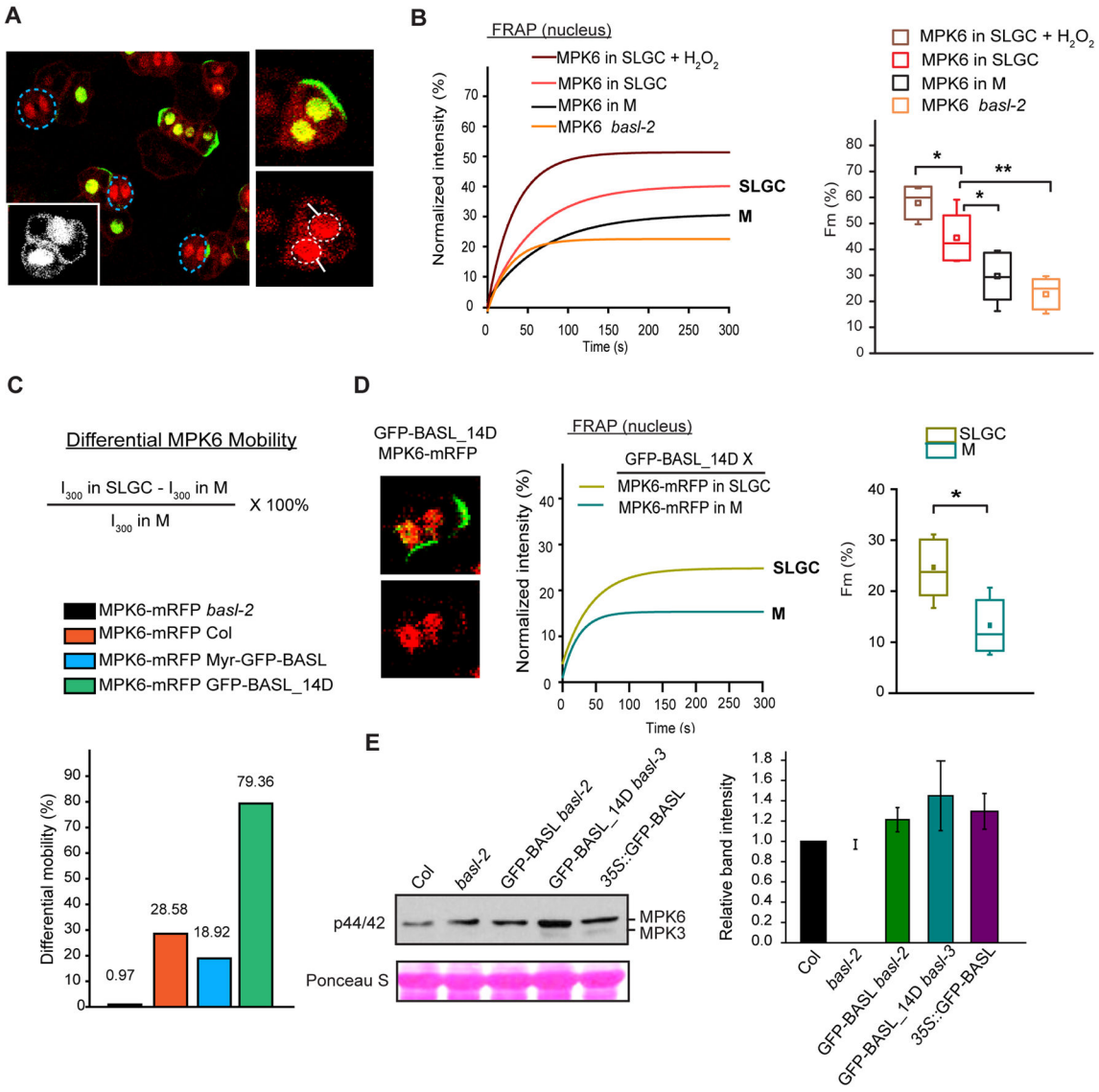

Figure 3. Differential MAPK Mobility in Two Daughter Cells Depends on the Presence of *BASL*

(A) Confocal images show subcellular localization of MPK6-mRFP (red and inset) driven by the *BASL* promoter in a 2-dpg adaxial cotyledon co-expressing GFP-BASL (green). FRAP assays were performed on nuclear mRFP-tagged MPK6 proteins in the Ms and in the SLGCs (white circles), respectively. Blue circles mark differentiating guard cells.

(B) Left: MPK6-mRFP FRAP curves in two daughter cells in WT *vs.* in *basl-2* and after H_2O_2 application. Right: the F_m values were used for statistical analysis. Mann–Whitney U test, ** $p < 0.01$; * $p < 0.05$.

(C) Quantification of differential MPK6 mobility in two daughter cells. Top: equation for calculating differential mobility of nuclear MPK6. Bottom: histograms show differential MPK6 mobility in various *BASL* backgrounds

(D) FRAP curves and quantification of MPK6-mRFP recovery in the presence of GFP-BASL_14D. Significant difference is evaluated by the Mann–Whitney U test, * $p < 0.05$.

(E) Western blots evaluate MPK3/6 kinase activity in designated genetic backgrounds. Twenty micrograms of total proteins from 3-dpg seedlings were used for detection of active MPK3 and MPK6 by a p44/42 MAPK antibody. Protein loading is visualized by Ponceau S staining. Histograms show quantification of MPK6 activity in different BASL backgrounds (n = three replicates).

See also Figure S3 and Table S1.

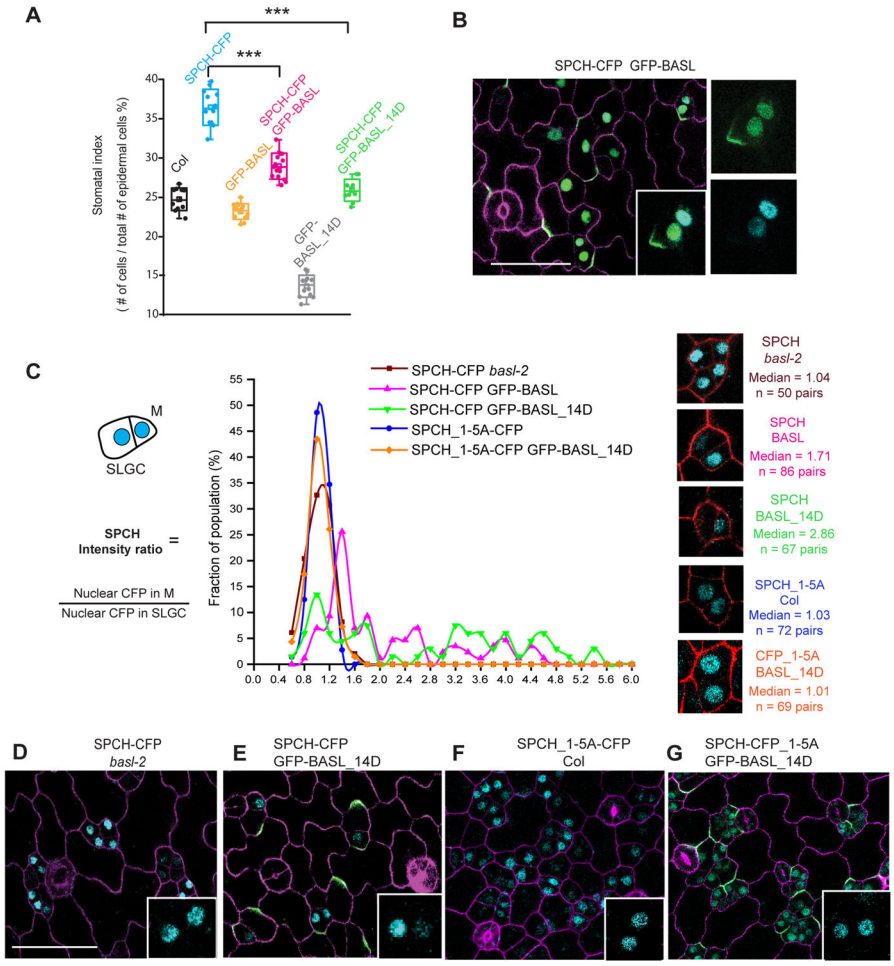

Figure 4. Polarized BASL Suppresses SPCH Expression in the SLGCs

(A) Box plots show quantification of stomatal index. The SI of SPCH-CFP was 36.4% (n = 2801 cells), compromised to 29% (n = 3503 cells) by GFP-BASL co-expression, and further reduced to 26% (n = 1874 cells) by GFP-BASL_14D. *** indicates significant differences relative to SPCH-CFP (Mann–Whitney U test, $p < 0.0001$).

(B) Left: confocal images show co-expression of SPCH-CFP (cyan) and GFP-BASL (green) in a 2-dpg cotyledon (Z-projection). Inset shows a magnified ACD pair, with respective GFP and CFP channel presented on the right. Note equivalent GFP intensity in two daughter cells but lowered CFP intensity in the SLGC.

(C) Quantification of differential SPCH levels in two daughter cells in designated *BASL* backgrounds. Left: quantification for differential expression of SPCH-CFP. Middle: histograms demonstrate SPCH-CFP intensity ratio in *basl*-2, GFP-BASL and GFP-BASL_14D plants, and SPCH_1-5A-CFP (a MAPK-insensitive version) in WT and in GFP-BASL_14D. n = 50–86 pairs of cells was measured for each category. The CFP intensity ratios were subject to histogram plotting with a bin size of 0.2. The Kolmogorov-Smirnov test showed that CFP intensity in the co-expression lines (SPCH-CFP GFP-BASL and SPCH-CFP GFP-BASL_14D) is significantly different from SPCH-CFP *basl*-2 ($p = 0$ and $p = 0.001$, respectively), but that of SPCH_1-5A-CFP in WT is not different from in GFP-

BASL_14D (p = 0.137). The median values and representative cells were presented on the right side. The mode values can be found in Table S3.
(D–G) Confocal images display SPCH-CFP (cyan) in *basl-2* (D) and co-expression with GFP-BASL_14D (green) (E), and SPCH_1-5A-CFP (cyan) in WT (F) and co-expression with GFP-BASL_14D (G). The insets show representative SPCH-CFP in two daughter cells. Note the severely suppressed SPCH-CFP when GFP-BASL_14D was co-expressed. Scale bar = 25 μm. (D–G) are at the same scale.
See also Figure S4.